Future Generation of Communication and Internet of Things (FGCIOT)

Journal homepage: http://fgciot.semnaniau.ac.ir/

PAPER TYPE (Research paper)

Magnetic and Structural Properties of CuO and Mn/Fe-Doped CuO Nanosheets for Nanomagnetic Device Applications

Hasan Khaleghi

Department of Physics, Se.C., Islamic Azad University, Semnan, Iran

Article Info

Article History:
Received: 12 June 2025
Revised: 5 August 2025
Accepted: 26 August 2025

Keywords:
Mn/Fe-doped in CuO, Nanosheets, hydrothermal method, Magnetic and Structural Properties, paramagnetic behavior, ferromagnetic properties

*Corresponding Author's Email Address: Hakh1355@iau.ac.ir

Abstract

In this study, CuO and $Cu_{0.92}Mn_{0.02}Fe_{0.06}O$ nanosheets were synthesized via the hydrothermal method. X-ray diffraction (XRD) was employed to characterize the structural features of the samples, while field-emission scanning electron microscopy (FESEM), elemental mapping (Map), and energy-dispersive X-ray spectroscopy (EDS) were used to investigate their surface morphology. The magnetic properties of the samples were examined using a vibrating sample magnetometer (VSM).

The results of quantitative and qualitative analyses revealed that both samples grew in nanosheet form and exhibited a monoclinic structure with the C2/c space group. Magnetic measurements indicated that pure CuO exhibits paramagnetic behavior, whereas the Mn- and Fe-doped compound $Cu_{0.92}Mn_{0.02}Fe_{0.06}O$ demonstrates ferromagnetic properties.

Introduction

In recent years, the study of materials with nanoscale structures has attracted considerable attention from researchers. The simultaneous combination of semiconducting and magnetic properties in semiconductor oxides makes them highly efficient candidates for processes such as dye degradation [1]. Among this class of metal oxides, copper oxide (CuO) nanoparticles have gained particular importance due to their non-toxicity and low production cost. At the nanoscale, CuO is a p-type semiconductor with a monoclinic crystal structure, exhibiting diverse applications in fields such as antimicrobial agents, lithium-ion batteries, and solar cells [2].

Doping CuO with transition metals, particularly iron (Fe), induces significant modifications in its magnetic, electrical, and optical properties [3]. To date, various methods have been developed for the synthesis of nanostructured semiconductor oxides, including microwave-assisted synthesis, hydrothermal methods, sputtering, electrochemical deposition, sol–gel processing, and co-precipitation [4].

In the present study, the hydrothermal method was employed to synthesize the samples. The crystal structure of the synthesized compounds was examined using X-ray diffraction (XRD). In addition, their morphology was analyzed by field-emission scanning electron microscopy (FESEM), elemental mapping, and energy-dispersive X-ray spectroscopy (EDS). The magnetic properties were further investigated using a vibrating sample magnetometer (VSM).

Experimental Work

A. Preparation

For the hydrothermal synthesis of CuO (abbreviated as CO) and $Cu_{0.92}Mn_{0.02}Fe_{0.06}O$ (abbreviated as CM2F6O), copper (II) nitrate trihydrate [$Cu(NO_3)_2{\cdot}3H_2O$], iron (III) nitrate nonahydrate [$Fe(NO_3)_3{\cdot}9H_2O$], and manganese (II) nitrate tetrahydrate [$Mn(NO_3)_2{\cdot}4H_2O$] were used as precursors. The precursors were dissolved in 40 mL of deionized water according to the calculated

Doi:

stoichiometric ratios, and the resulting solution was stirred at room temperature for 20 minutes using a magnetic stirrer.

Subsequently, potassium hydroxide (KOH) solution was gradually added to the initial solution until a final concentration of 0.5 M was achieved. The mixture was stirred magnetically for an additional 6 hours and then transferred to an autoclave. The hydrothermal process was carried out at 160 °C for 3 hours.

After removal from the autoclave, the precipitate was washed several times with deionized water. To ensure neutral pH, the washing process was repeated using centrifugation. Finally, the product was dried at 80 °C for 6 hours, yielding black CuO and $Cu_{0.92}Mn_{0.02}Fe_{0.06}O$ powders.

Results and Discussion

A. X-ray Diffraction (XRD)

The crystal structures of the samples, as determined by X-ray diffraction, are shown in Fig. 1. For the CuO sample, a monoclinic structure with space group C2/c (reference code: 00-048-1548) was obtained. The $Cu_{0.92}Mn_{0.02}Fe_{0.06}O$ sample exhibited the same structure. Since the ionic radii of Fe and Mn are smaller than that of Cu, these ions readily substituted Cu ions within the CuO crystal lattice without altering its monoclinic structure.

The XRD patterns of the samples display two major peaks corresponding to the (111) and (–111) planes. The CuO sample is single-phase and free of impurities, as shown in the figure.

The refinement results are presented in Fig. 2, and the corresponding crystallographic parameters are summarized in Table 1. To obtain lattice constants (a, b, and c), β angle, and unit cell volume (V) of all the samples, the FullProf software was used. The refinement results are presented in Fig. 2, and the corresponding crystallographic parameters are summarized in Table 1. As one can infer, the network constant, β angle and V of the CuO sample are in an acceptable agreement with the standard monoclinic structure of the CuO (a = 4.6883 Å, b = 3.4229 Å, c = 5.1319 Å, β = 99.50600, and V = 81.22 $Å^3$). Generally, these results indicate a reasonable agreement between the experimental and the theoretical data.

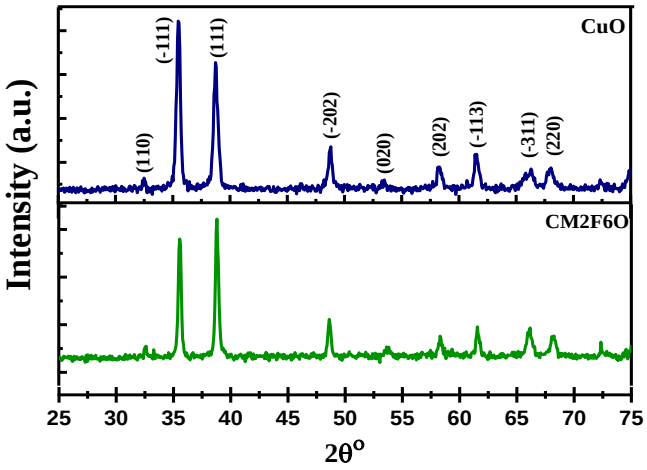

Fig. 1: X-ray diffraction (XRD) patterns of the samples.

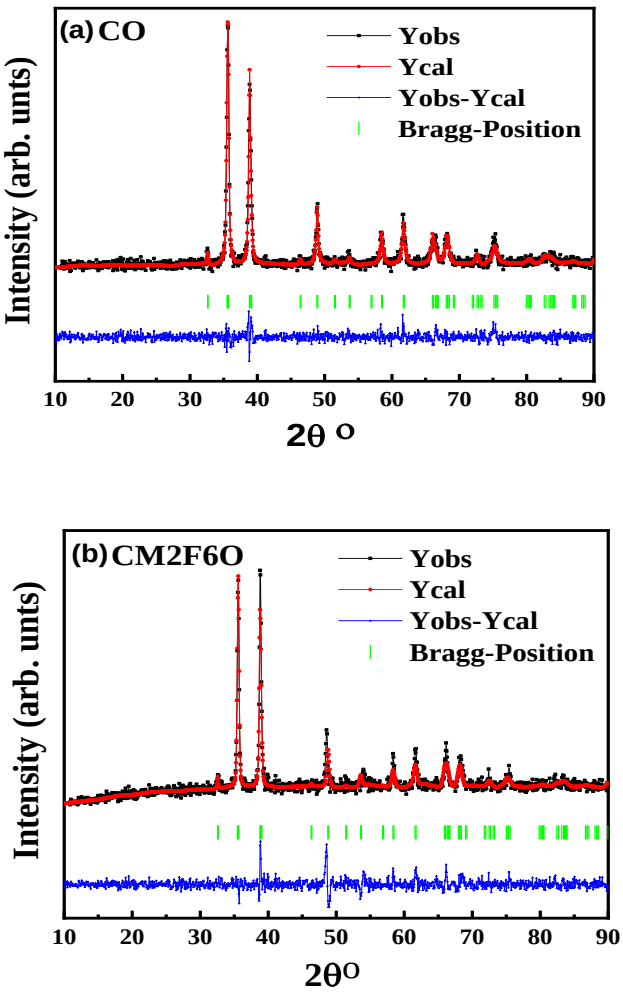

Fig. 2: Rietveld refinement analysis of the samples.

Table 1: Lattice parameters, unit cell volume, and goodness-of-fit (GOF).

Sample	**CO**	**CM2F6O**
Space group	C2/c	C2/c
structure	Monoclinic	Monoclinic
a(A°)	4.6730	4.6829
b(A°)	3.4140	3.4177
c(A°)	5.1240	5.1300
α	90	90
β	99.496	99.498
γ	90	90
GOF	1.24	1.67
V (Å³)	80.6262	80.9768

B. Surface Morphology

FESEM images at a magnification of 100 nm along with elemental mapping are shown in Fig. 3. The CuO nanosheets clearly exhibit diverse dimensions. Upon the incorporation of Fe, the morphology of the nanosheets in the $Cu_{0.92}Mn_{0.02}Fe_{0.06}O$ sample changes, becoming more irregular and sharper in appearance.

The EDS results for the samples are summarized in Table 2. These results confirm the absence of any secondary phases in the samples. The additional Au peaks observed in the spectra are attributed to the gold coating applied to the nanosheets during the EDS analysis.

As an example, the elemental mapping analysis of the $Cu_{0.92}Mn_{0.02}Fe_{0.06}O$ sample is presented in Fig. 4. The mapping results demonstrate a uniform distribution of Fe, Mn, O, and Cu elements within the sample. This indicates that the dopant elements are well incorporated into the lattice, leading to the formation of a structure with minimal lattice defects. The same conclusion also holds for the CuO sample.

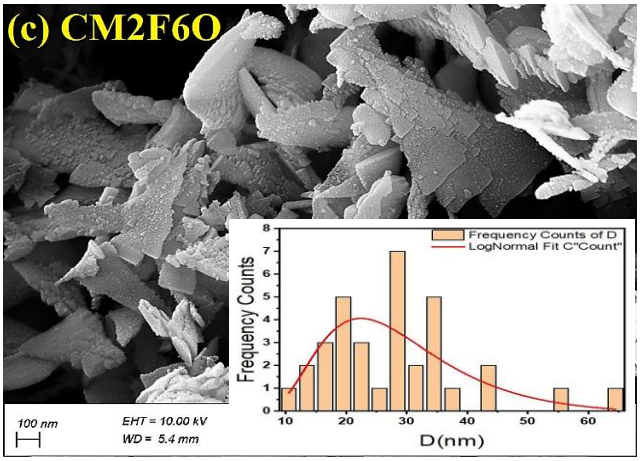

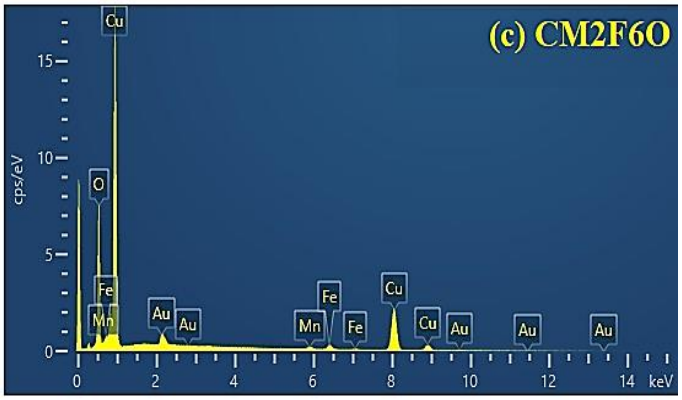

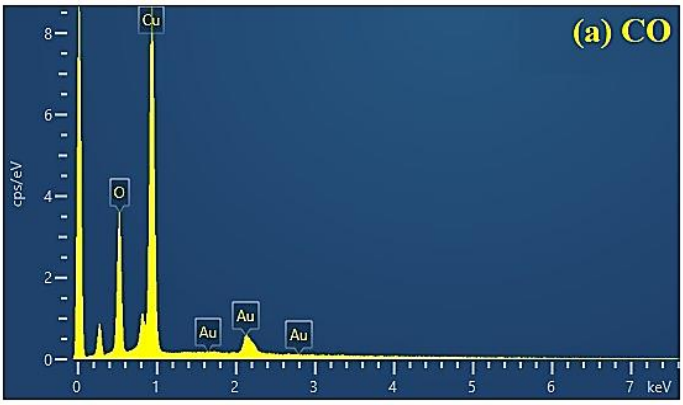

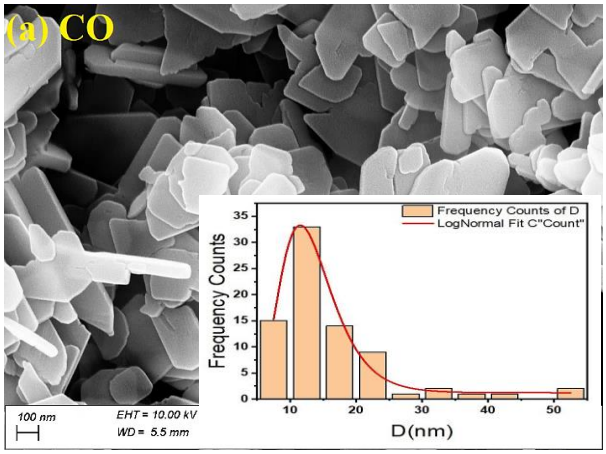

Fig. 3: FESEM images and EDS spectra of the samples.

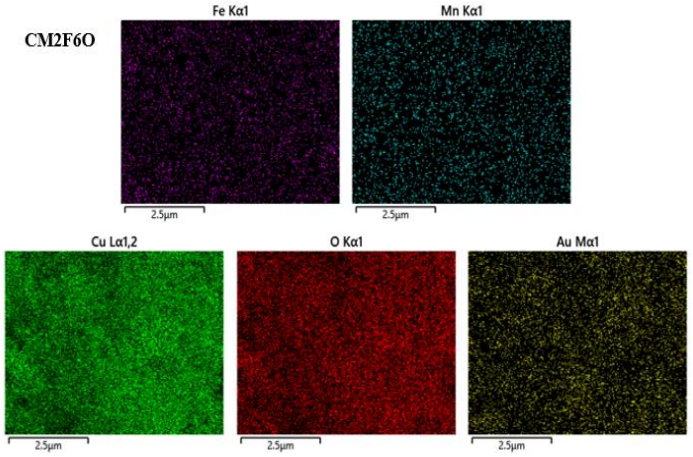

Fig. 4: Elemental mapping images of the CM2F6O sample.

The thickness of the nanosheets in the samples was measured using the DigiMizer software. The data were plotted as a histogram and fitted with the following exponential function [5] (see Appendix, Fig. 3):

$$f(D) = \left(\frac{1}{\sqrt{2\pi}\sigma \cdot D}\right)\exp\left[-\frac{ln^2\left(\frac{D}{D_0}\right)}{2\sigma^2}\right] \quad (1)$$

By determining D_0 and σ from the obtained plot, the average nanosheet thickness <D> and the standard deviation σ_D were calculated using the following equations and are listed in Table 2 [6]:

$$< D >= D_0 \exp\left(\sigma^2/_2\right) \quad (2)$$

$$\sigma_D = < D > [exp(\sigma^2) - 1]^{1/_2} \quad (3)$$

Table 2: Average nanosheet thickness and atomic percentages of elements in the samples.

sample	CO	CM2F6O
DFESEM $\pm\sigma_D$	13.64±4.70	29.77±13.60
O (Atomic %)	57.30	58.31
Cu (Atomic %)	42.70	39.45
Fe (Atomic %)	-	1.55
Mn (Atomic %)	-	0.69

C. Magnetic Properties

The room-temperature M–H hysteresis curves of the samples, measured under a high magnetic field of ±20 kOe, are shown in Fig. 5. The hysteresis curve of the CuO sample exhibits typical paramagnetic behavior, a characteristic previously reported for copper oxide [1, 7].

Upon incorporation of Fe, the hysteresis curve of the $Cu_{0.92}Mn_{0.02}Fe_{0.06}O$ sample displays ferromagnetic behavior [8]. The paramagnetic behavior of CuO is attributed to superexchange interactions among the lattice ions, whereas the ferromagnetic behavior observed in $Cu_{0.92}Mn_{0.02}Fe_{0.06}O$ arises from FCE (ferromagnetic coupling exchange) interactions between the ions and oxygen vacancies.

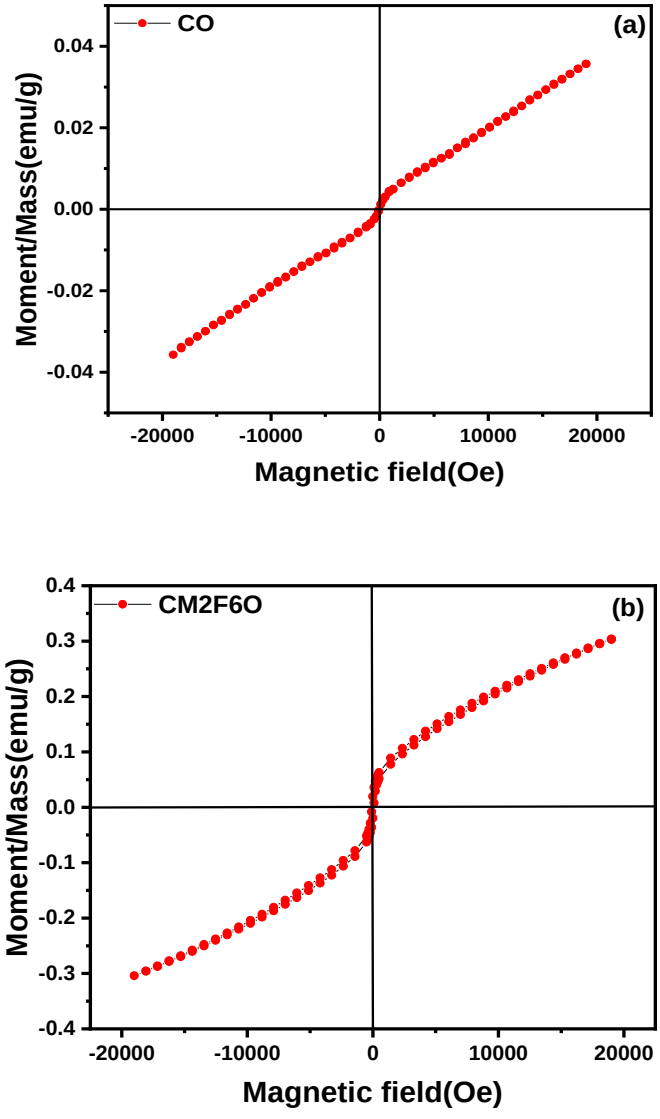

Fig. 5: Room-temperature M–H hysteresis curves of the samples.

Conclusion

In this study, the effect of partial substitution of Fe and Mn on the structure and properties of CuO nanosheets was investigated. X-ray diffraction results revealed that

the monoclinic structure of CuO remains unchanged in the presence of Fe and Mn, and that Fe ions successfully substitute Cu ions in the lattice. Rietveld analysis and FESEM images confirmed that the samples are single-phase, free of impurities, and that the elements are uniformly distributed within the crystal lattice.

The incorporation of Fe altered the morphology of the nanosheets, making them more irregular and sharper, while the average nanosheet thickness was measured and found to follow a predictable distribution. Magnetic studies indicated that pure CuO exhibits paramagnetic behavior, whereas Fe substitution induces ferromagnetic behavior, attributed to ferromagnetic coupling exchange (FCE) interactions between the ions and oxygen vacancies.

Conflict of Interest

The author declares that there is no conflict of interests regarding the publication of this manuscript. In addition, the ethical issues, including plagiarism, informed consent, misconduct, data fabrication and/or falsification, double publication and/or submission, and redundancy have been completely observed by the authors.

Abbreviations

CuO	Copper oxide
Mn	Manganese
Fe	Iron
XRD	X-ray diffraction
FESEM	Field-emission scanning electron microscopy
EDS	Energy-dispersive X-ray spectroscopy
Map	Elemental mapping
VSM	Vibrating sample magnetometer
CO	CuO
CM2F6O	$Cu_{0.92}Mn_{0.02}Fe_{0.06}O$
KOH	Potassium hydroxide
a, b, and c	lattice constants
α, β, and γ	lattice angles

References

[1] E. Swatsitang, A. Karaphun, and T. Putjuso, "Influence of Fe: Co co–doping on the morphology, optical and magnetic properties of Cu1-(x+ y) FexCoyO nanostructures prepared by a hydrothermal method," Physica B: Condensed Matter, vol. 583, p. 412044, 2020.

[2] M. Shahmiri, N. A. Ibrahim, W. M. Z. W. Yunus, K. Shameli, N. Zainuddin, and H. Jahangirian, "Synthesis and characterization of CuO nanosheets in polyvinylpyrrolidone by quick precipitation method," Advanced Science, Engineering and Medicine, vol. 5, no. 3, pp. 193-197, 2013.

[3] B. P. Singh et al., "Effect of Co and Mn doping on the morphological, optical and magnetic properties of CuO nanostructures," Solid State Sciences, vol. 106, p. 106296, 2020.

[4] A. Joseph et al., "An experimental investigation on pool boiling heat transfer enhancement using sol-gel derived nano-CuO porous coating," Experimental Thermal and Fluid Science, vol. 103, pp. 37-50, 2019.

[5] M. Ehsani, S. Esmaeili, M. Aghazadeh, P. Kameli, and I. Karimzadeh, "Magnetic evaluation of the nanoparticles coated with polyvinylpyrrolidone and polyvinyl chloride nanoparticles synthesized by electro-deposition method for hyperthermia application," Journal of Superconductivity and Novel Magnetism, vol. 32, no. 7, pp. 2021-2030, 2019.

[6] S. Esmaeili, M. Ehsani, and M. Fazli, "Photo-catalytic activities of La0. 7Ba 0.3 MnO3 nanoparticles," Optik, vol. 216, p. 164812, 2020.

[7] B. P. Singh et al., "Effect of Co and Mn doping on the morphological, optical and magnetic properties of CuO nanostructures," Solid State Sciences, vol. 106, p. 106296, 2020.

[8] J. Coey, A. Douvalis, C. Fitzgerald, and M. Venkatesan, "Ferromagnetism in Fe-doped SnO 2 thin films," Applied Physics Letters, vol. 84, no. 8, pp. 1332-1334, 2004.